ADVANCED HEALTHCARE MATERIALS
www.advhealthmat.de

Neuronal Migration on Silicon Microcone Arrays with Different Pitches

Jeongyeon Seo, Christina Lanara, Ji Yu Choi, Jungnam Kim, Hyeoncheol Cho, Young-Tae Chang, Kyungtae Kang, Emmanuel Stratakis, and Insung S. Choi**

Special issue dedicated to George M. Whitesides

Neuronal migration is a complicated but fundamental process for proper construction and functioning of neural circuits in the brain. Many in vivo studies have suggested the involvement of environmental physical features of a neuron in its migration, but little effort has been made for the in vitro demonstration of topography-driven neuronal migration. This work investigates migratory behaviors of primary hippocampal neurons on a silicon microcone (SiMC) array that presents 14 different pitch domains (pitch: 2.5–7.3 µm). Neuronal migration becomes the maximum at the pitch of around 3 µm, with an upper migration threshold of about 4 µm. Immunocytochemical studies indicate that the speed and direction of migration, as well as its probability of occurrence, are correlated with the morphology of the neuron, which is dictated by the pitch and shape of underlying SiMC structures. In addition to the effects on neuronal migration, the real-time imaging of migrating neurons on the topographical substrate reveals new in vitro modes of neuronal migration, which have not been observed on the conventional flat culture plate, but been suggested by in vivo studies.

Neuronal migration is one of the most crucial steps in the construction of the nervous system. In the embryonic period, newborn neurons migrate to reach their appropriate positions.[1–3] The migration processes continue, after birth, to establish and maintain the neural circuitry. Studies on the underlying mechanisms, which initiate and guide the migration of neurons at the proper moment, have suggested the role of environmental cues. Since Rakic reported the neuronal migration along the processes of radial glial cells—radial migration[4,5]—in 1971,[6] the importance of environmental physical features for a neuron in its migration has been remarked upon again, as Weiss had suggested in 1934.[7] In the radial migration, the aligned leading neurites of migrating neurons are often enveloped by glial appendages, indicating dynamic, reciprocal interactions between neurons and glial fibers. In vivo neurons also migrate in a different mode: in the tangential migration,[8–10] neurons often move in a direction orthogonal to the glial fibers and cooperate with radially migrating neurons in corticogenesis. Because the tangential migration is defined as a mode of nonradial neuronal translocation, neighboring cells,[11] like radial glial fibers in radial migration, were suggested to act as substrates on which the neurons migrate. Directly contacting cells or blood vessels[12] would provide topographical cues to tangentially migrating neurons in vivo, along with biochemical cues, but it still remains unknown whether spatial, physical structures actively contribute to the biological control of neuronal migration.

Previous in vitro studies have elucidated topographical effects on several neuronal behaviors including neuronal adhesion,[13,14]

J. Seo, Dr. J. Y. Choi, J. Kim, H. Cho, Prof. I. S. Choi
Center for Cell-Encapsulation Research
Department of Chemistry
KAIST
Daejeon 34141, Korea
E-mail: ischoi@kaist.ac.kr

C. Lanara, Dr. E. Stratakis
Institute of Electronic Structure and Laser
Foundation for Research and Technology Hellas (FORTH)
Nikolaou Plastira 100 Heraklion, Crete GR-70013, Greece
E-mail: stratak@iesl.forth.gr

Prof. Y.-T. Chang
Department of Chemistry
POSTECH
Center for Self-Assembly and Complexity
Institute for Basic Science (IBS)
Pohang 37673, Korea

Prof. K. Kang
Department of Applied Chemistry
Kyung Hee University
Yongin Gyeonggi 17104, Korea

Prof. I. S. Choi
Department of Bio and Brain Engineering
KAIST
Daejeon 34141, Korea

The ORCID identification number(s) for the author(s) of this article can be found under https://doi.org/10.1002/adhm.202000583

DOI: 10.1002/adhm.202000583

neurite outgrowth,[15–18] and network formation.[19,20] The interrelation between the direction of neurite elongation and the topographical feature has enormously been studied.[21–23] The concept of contact guidance has been proposed to explain the direction of neurite elongation depending on the type of neurons and the morphological attributes of topography.[24–27] Neuritogenesis and neurite outgrowth were greatly accelerated on nanotopographical substrates.[15,28–31] A new in vitro developmental pathway for hippocampal neurons has even been reported on nanotopography.[32] Despite recent remarkable findings, it is the topographical influences on neuronal migration that remain as one of the missing pieces in understanding of neuronal development on various surface topographies. Neuronal migration on substrates with different topographies has rarely been discussed,[33] although thetopographical roles in neuronal migration were suggested to exist by the in vivo studies, and the general roles of subcellular components, such as organelles and cytoskeletons, during migration have been identified in vitro.[34–38] As aforementioned, neurons respond to topographical features and show different functional events during their early development, compared with those on flat culture substrates,[32,39] which suggests the possibility that the topographical features could also affect the migration of neurons, as they affect other cell types.[40–44] Herein we report the migration behaviors and morphological changes of primary hippocampal neurons on a microstructured culture platform with different pitches.

The silicon microcone (SiMC) array with different pitches was fabricated by a Ti:Sapphaire femtosecond laser system (Figure S1, Supporting Information).[45,46] In this paper, we define the pitch as the distance between peaks of adjacent microcones. The controlled laser-parameters, with a computer-driven X-Y transition stage, enabled the generation of step-gradient pitches, composed of 14 different domains (P1–P14), by varying the laser fluence from 0.17 to 0.78 J cm^{-2} (Table S1, Supporting Information). The field-emission scanning electron microscopy (FE-SEM) images of the SiMC array, with top and tilted (45°) views, showed that the pitch and roughness (i.e., height) of microcones increased gradually, and the major axes of the elliptical microcones were parallel to the step-gradient axis (**Figure 1**a). The width of each domain was set to be 500 µm, and the fabricated SiMC array, containing 14 domains, was 7 mm wide and 4 mm high. Pitches in the step-gradient axis and roughnesses varied from 2.54 ± 0.55 (P1) to 7.25 ± 1.25 µm (P14) in pitch and from 2.66 ± 0.32 (P1) to 11.33 ± 1.98 µm (P14) in roughness (**Table 1**).

Primary hippocampal neurons dissociated from embryonic day 18 (E18) Sprague-Dawley rat hippocampi were cultured on the SiMC array after coating with laminin.[47,48] Neuronal nuclei were fluorescently labeled with Hoechst 33342 at 3 h of culture, when the neurons stably adhered to the substrate, and tracked every 15 min from 4 to 12 h of culture by confocal laser-scanning microscopy (CLSM). The nucleus positions on the SiMC array were digitized into the x and y coordinates by using the TrackMate plugin of Image J, and the neuronal migration was followed by linking the time-evolved positions for each nucleus. Based on the preprocessed data, we calculated the total migration distance and the averaged migration speed (the total migration distance divided by 8 h). Analysis on the migration speed on one and every pitch domain (from P1 to P14) arguably confirmed that the pitches of the SiMC array indeed significantly affected the behavior of neuronal migration (Table 1 and Figure 1b). The highest migration speed was observed on the P3 domain, the pitch of which was 3.21 ± 0.76 µm. The migration speed decreased with pitch changes and leveled off beyond P7 (pitch: 4.11 ± 0.85 µm). As a comparison, the speed dropped to about 45% on P7 from that on P3 (16.56 µm h^{-1} on P3 vs 9.17 µm h^{-1} on P7). The results suggested the existence of an upper threshold for topography-driven, in vitro neuronal migration in the micrometer scale.

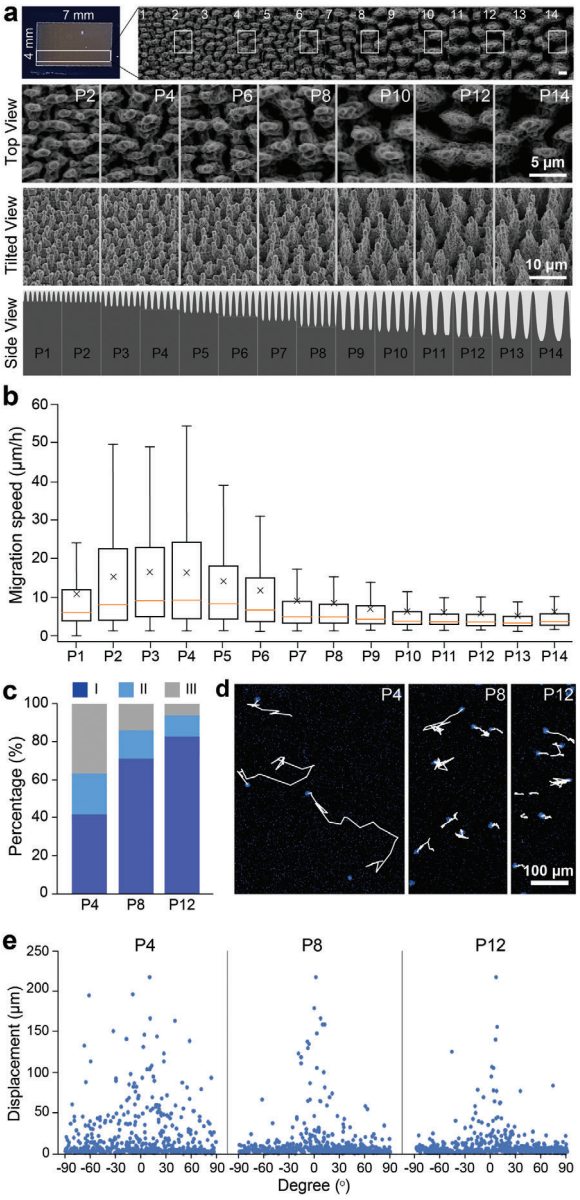

Figure 1. a) FE-SEM micrographs of different pitch domains (from P1 to P14) in the SiMC array, with a side-view schematic of the microcones. b) A box-and-whisker plot of neuronal-migration speed on each pitch domain. c) Percentages of the migrating neurons for Groups I, II, and III on P4, P8, and P12. d) CLSM images of the somata (blue) on P4, P8, and P12, with their trajectory lines (white). e) Scatterplots of neuronal displacement and angle degree of displacement for P4, P8, and P12.

Table 1. Pitches, roughnesses of and neuronal-migration speeds on the pitch domains (P1–P14) of the SiMC array.

Domain	Pitch [μm]	Roughness [μm]	Speed [μm h^{-1}]
P1	2.54 ± 0.55	2.66 ± 0.32	10.85
P2	3.04 ± 0.59	2.96 ± 0.45	15.53
P3	3.21 ± 0.76	3.27 ± 0.41	16.56
P4	3.30 ± 0.48	3.66 ± 0.39	16.41
P5	3.77 ± 0.74	4.16 ± 0.40	14.10
P6	3.88 ± 0.70	4.30 ± 0.61	11.83
P7	4.11 ± 0.85	5.08 ± 0.70	9.17
P8	4.20 ± 0.74	5.50 ± 0.91	8.51
P9	4.80 ± 0.84	5.47 ± 0.81	7.07
P10	4.97 ± 0.94	7.19 ± 1.46	6.20
P11	5.37 ± 0.84	7.33 ± 1.35	6.14
P12	5.62 ± 1.14	9.49 ± 1.22	5.75
P13	6.39 ± 1.22	11.43 ± 1.73	5.25
P14	7.25 ± 1.25	11.33 ± 1.98	6.25

With P4 (pitch: 3.30 ± 0.48 μm), P8 (pitch: 4.20 ± 0.74 μm), and P12 (pitch: 5.62 ± 1.14 μm) as representatives of small, medium, and large pitches (Figure S2, Supporting Information), further analysis was made by grouping the neurons into three categories based on their total migration distance (I: <50 μm; II: ≥50 μm and ≤100 μm; III: >100 μm) (Figure 1c). The migration distances of at least 190 neurons were measured for each pitch domain in the time-lapse CLSM images. Although the neurons were somewhat heterogeneous in terms of migration distance, the analysis clearly indicated that actively moving neurons (i.e., neurons in Group III) were more popular on P4 than on P8 and P12. The migration distance displayed a non-Gaussian distribution, but a higher percentage of the neurons moved more than 50 μm on P4, compared with P8 and P12. Quantitatively, 58.28% of the neurons were categorized to Groups II or III in the case of P4, and the percentage decreased to 29.14% and 17.67% for P8 and P12, respectively. The percentage of Group III for P4 was even higher than the percentage sum of Groups II and III for P8 or P12. On P8 and P12, more than 70% of the neurons moved less than 50 μm. It is to note that the pitch difference of ≈0.9 μm between P4 and P8 led to the significant differences in group-percentage distribution and migration speed: Group I (41.72%), Group II (21.41%), Group III (36.87%), and speed (16.41 μm h^{-1}) on P4; Group I (70.86%), Group II (15.18%), Group III (13.96%), and speed (8.51 μm h^{-1}) on P8.

In addition to the migration speed, the morphology of neurons is another feature related to their migration. For example, migrating neurons generally take a bipolar morphology that has leading and trailing neurites in directions opposite to each other.[49,50] We counted the number of neurites sprouting from the soma and observed more bipolar neurons on P4 (47.44%) than on P12 (26.62%). The values were roughly similar to the percentage sum of Groups II and III, additionally supporting that more neurons were active on P4 in the aspect of their migration (Figure S3, Supporting Information). The trajectory plots in neuronal movement indicated that the majority of neuronal-migration directions seemed to be in parallel to the step-gradient axis (i.e., horizontal migration in the images) (Figure 1d). For further analyses, we generated the scatterplot of migration displacement (i.e., the distance between initial and final locations of a nucleus in 8 h) versus angle degree of the displacement (0°: the step-gradient axis) for each pitch domain (Figure 1e). Of interest, nearly all the displacement of more than 50 μm on P8 and P12 were between −30° and 30° of angle degree, and the parallel displacement was more discernable in the case of P12. In comparison, the neuronal movement was more scattered on P4 in the aspect of angle degree.

The direction of neurite elongation, especially that of leading neurites, generally determines the direction of neuronal migration, locomotion, and translocation.[51–53] In this study, we characterized the cytoskeletal structures, such as microtubules and actins, after fluorescent staining, for obtaining the information on neurite directionality. In conjunction with the neurite directionality, the direction of neuronal migration was also investigated based on the movement of fluorescently stained nuclei. The neurite directionality was measured at 9 h of culture, and the migration angle was done for each neuronal migration between 4 and 12 h of culture. The CLSM images indicated that more neurites were aligned to the step-gradient axis on P8 and P12 than on P4 (**Figure 2**a), in agreement with our previous result showing the connection between direction of neurite elongation and elliptical SiMC structures.[54] The major-axis directionality of the elliptical SiMC structures was evaluated quantitatively, and the angle-distribution data showed that the majority was within ±15° to the step-gradient axis, indicating the neurite elongation in parallel to the major axis of the SiMC (Figure S4, Supporting Information). The detailed analysis showed that the neurons on P4 did not extend the neurites only in the parallel direction (0°), but tended to do in both parallel and diagonal (−45° and 45°) directions (parallel: 12.17% and diagonal: 8.81%) (Figure 2b). The percentage of diagonally aligned neurites greatly decreased in the cases of P8 and P12, and the majority of neurite direction was in parallel to the step-gradient axis (P8: 25.38% and P12: 25.99%). This observation could be explained by our previous work in which the neurite orientations on the isotropic micropillar array were localized into the three axes (i.e., horizontal, vertical, and diagonal axes) with the interpillar distance of 3 μm.[18] It was also reported that increasing the interpillar distance of an axis to above 3 μm diminished the neurite alignment to the micropillar axis. In other words, the directional neurite-elongation had a threshold of ≈4 μm ($3\sqrt{2}$), with which the current data was in good agreement. On P4 did the neurons and their neurites have more directionality options for neuronal movement and neurite elongation than on P8 or P12. The angle degrees in migration on P4 were distributed more broadly in a symmetrical fashion with the maximum spike at 0°, implying that neuronal movement was connected closely with the neurite direction (Figure 2c). Taken together, it could be concluded that more options for neurite elongation and soma movement on P4 under the upper threshold led to the higher migration speed and longer migration distance than on P8 or P12. Our results also showed that the topographical features, such as pitches and shapes, critically affected various neuronal processes, including the speed and direction of neuronal movement as well as the direction of neurite elongation.

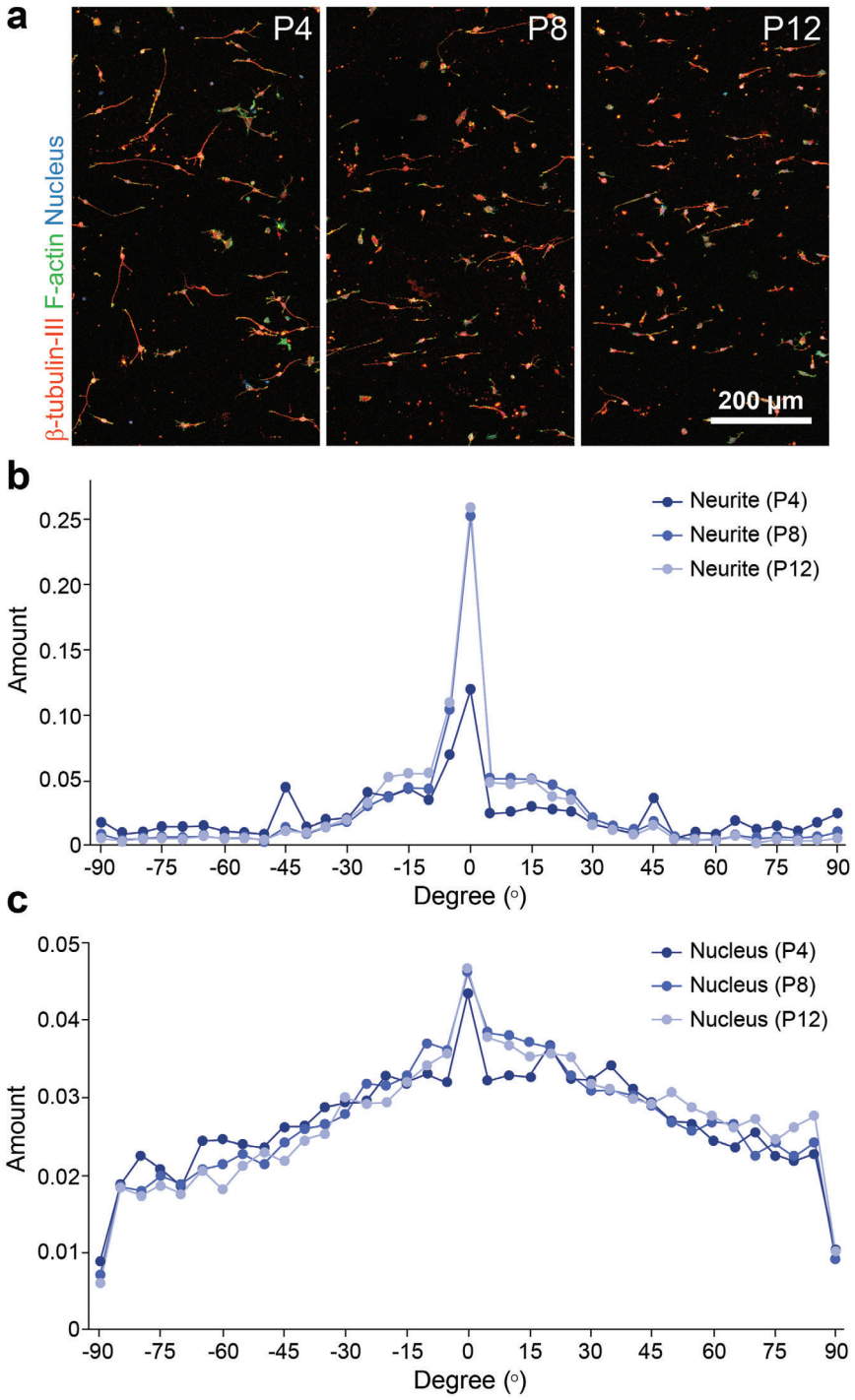

Figure 2. a) CLSM microscopy images of hippocampal neurons on P4, P8, and P12. Nucleus (blue); F-actin (green); *β*-tubulin III (red). Directionality of b) neurite elongation and c) neuronal migration on P4, P8, and P12.

We investigated the real-time morphology changes of the migrating neurons in our system, after staining with NeuO (a neuron-specific dye).[55] Previous reports generally described the in vitro morphology of migrating neurons and its changes, with suggested underlying mechanisms on the migrations including nuclear movement and leading-neurite extension.[34–36] However, the morphological dynamics of migrating neurons on topographically complex substrates is yet to be shown. The time-lapse CLSM images confirmatively showed a close relationship between neurite elongation and soma movement during neuronal migration (**Figure 3**). Some fast-migrating neurons had noticeable morphological changes during migration (Figure 3a).

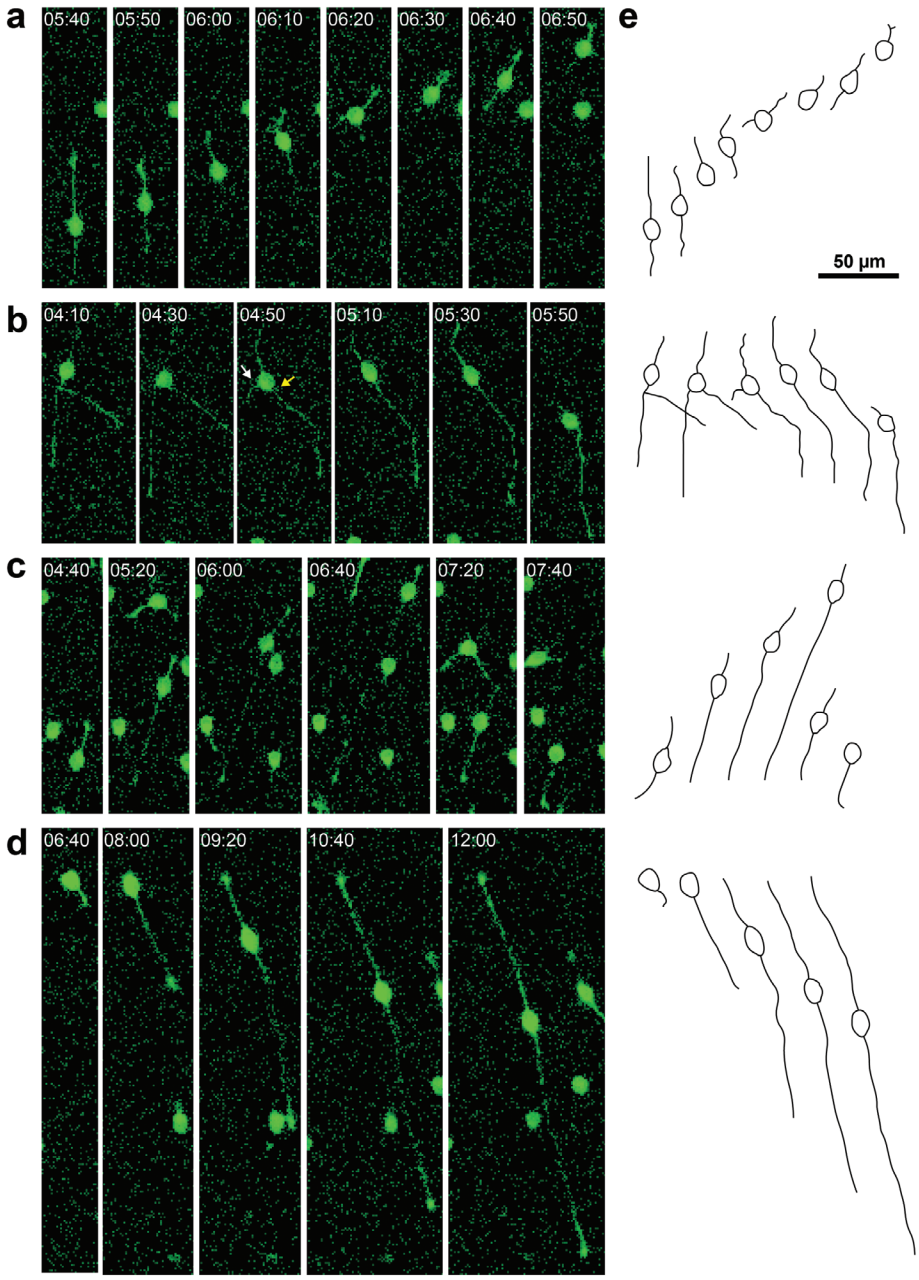

Figure 3. Time-lapse CLSM images of (left, a–d) migrating neurons on the SiMC array and (right, e) illustrations of their morphological changes during migration. The images in live-cell imaging were taken every 10 min. Neurons were stained by a neuron-specific dye, NeuO (green).

Neurons with short and unbranched leading neurites, reported as one of the features of in vivo neurons in locomotion,[53,56] dynamically sprouted and retracted the neurites with changes in length and position, until their somata moved toward the elongation direction of the leading neurite. The trailing neurites, sprouted oppositely to the leading neurites, became shorter, and in some cases, they were retracted completely. We also observed that some branched neurons showed unique morphological changes during the migration (Figure 3b). When the soma reached the branching point of the leading neurite, the complete retraction of one branch occurred (white arrow) along with the extension of the other branch (yellow arrow). The soma then migrated to the direction of the remaining extended branch, which was consistent with the previous in vitro studies, employing flat substrates, as well as in vivo ones.[57–59] These representative examples showed that the neurons on the microtopographical substrate, in some cases, exhibited the migration behaviors found in the neurons both on flat substrates andin vivo. In addition, the two types of neurons in Figure 3a,b showed the nonsaltatory continuous and conventional saltatory movements respectively (Figure S5, Supporting Information), supporting the hypothesis on the

coordination of multiple mechanisms for neuronal migration in vivo.[60]

On the SiMC array, several other neuronal behaviors were also found, which were not related with those on in vitro flat substrates. Since both extension of the leading neurites and retraction of the trailing neurites occur repeatedly during neuronal migration, the trailing neurites are generally not longer than the leading neurites on flat substrates. However, we observed that, in some cases for the SiMC array, the retraction of the trailing neurites was restrained, and the migrating bipolar neurons moved to the direction of the shorter leading neurites (Figure 3c). A careful analysis suggested that the tip of the neurite in the opposite direction of soma movement was physically pinned to the initial point during the migration, implying that the topography caused intimate interactions between the neurites and the substrate surface (Figure S6, Supporting Information).[61,62] As the soma moved toward the leading neurite, the pinned trailing neurite was physically extended and eventually became longer than the leading neurite. The soma reversed its moving direction and moved toward the longer pinned neurite, which had originally been the trailing neurite. As far as we know, this type of the pinned trailing neurite and the retrograde movement—the neurons reversely move to the direction of pinned trailing neurites—has only been observed in vivo with the newborn cortical neurons in the subventricular zone.[63] As a related work, neuronal migration with simultaneous extension of the longer neurite in the opposite direction has been reported for 3D cylindrical hydrogels with chemical gradient.[64] In other cases, the leading neurite was constantly longer than the pinned trailing neurite (Figure 3d). The initial point of the soma became a tip of the trailing neurite, when the soma moved. These morphological characteristics—the unbranched, simple leading neurite and the pinned trailing neurite—were reminiscent of the migrating cortical neurons in neocortical slice cultures.[65]

In summary, we showed that a physical cue—pitch of microcone substrates in our study—could be a crucial factor in neuronal migration and its speed. In the micrometer-scaled pitches, hippocampal neurons were most movable at the pitch of around 3 µm, and the neuronal migration decreased significantly at the pitches of above 4 µm, suggesting an upper threshold of 4 µm for neuronal migration. In addition, the topographical cues of the SiMC array induced the neuronal behavior during migration that had not been observed in vitro on flat substrates. The observed retrograde migration suggests that the tension, derived from pure topography,[66,67] would be sufficiently enough to induce the neuronal movement, suggesting the potential of topography in programmed control of neuronal behavior in vitro. We believe it feasible to tightly guide the neuronal migration via topotaxis[68] with technological development for fabrication of nanotopographical gradients and fully recapitulate in vivo behavior of neurons in the in vitro setting with synergistic combination of biochemical and topographical cues.

Experimental Section

Materials: Neurobasal medium (Gibco), B-27 supplement (50 ×, Gibco), GlutaMAX (100 ×, Gibco), laminin (Sigma-Aldrich), L-glutamic acid (Sigma-Aldrich), penicillin-streptomycin (5000 U mL^{-1} of penicillin and 5000 µg mL^{-1} of streptomycin, Welgene), phosphate-buffered saline (10 × PBS, pH 7.2, Welgene), Hank's balanced salt solution (HBSS, Welgene), paraformaldehyde (Sigma-Aldrich), bovine serum albumin (BSA, Sigma-Aldrich), anti-β-tubulin III rabbit polyclonal antibody (Sigma-Aldrich), Alexa Fluor 594 goat anti-rabbit IgG secondary antibody (Invitrogen), Alexa Fluor 488phalloidin (Invitrogen), antifade mounting medium with 4,6-diamidino-2-phenylindole (DAPI, Vector laboratories), glutaraldehyde solution (Sigma-Aldrich), and hexamethyldisilazane (HMDS, Sigma-Aldrich) were used as received. Deionized (DI) water was obtained from a Human Ultra Pure System (Human Corp.).

Fabrication of SiMC Arrays: An n-type Si(100) wafer was subjected to ultrashort femtosecond laser irradiation. The Ti:Sapphire laser system based on chirped pulse amplification (CPA) technique, which used the directly diode-pumped, ytterbium-doped potassium gadolinium tungstate (Yb:KGW) crystal as an active medium, produced linearly polarized pulses of 170 fs duration, 1 kHz repetition rate, and 1026 nm central wavelength. The laser beam, entering the processing chamber through a quartz entrance window, was focused by a 40 cm focusing plano convex lens onto the sample surface. The whole process took place in a vacuum chamber, where the pressure of the background sulfur hexafluoride (SF_6) gas was maintained to be 350 mbar. For areal scanning, the chamber was placed on a computer-driven *X*–*Y* translation stage. A motorized rotation stage with neutral density filter was used to achieve smooth beam power transitions. Linescan separation was stable on 20 µm, and rotational stage step was stable on 1.1°. The laser fluence was varied from 0.17 to 0.78 J cm^{-2} to produce gradually increasing 14 pitches with width of 500 µm each. The irradiation process was visualized through a plexiglas window, which was laterally mounted on the vacuum chamber. After laser treatment, the samples were cleaned in aqueous hydrofluride dilution for 60 min and dried by blowing nitrogen gas. Finally, the micropatterned silicon substrate was thermally oxidized at 1000 °C for 90 min in air. The thermal treatment formed a conformal silicon oxide layer with thickness of 100 nm.

Neuron Culture: Primary hippocampal neurons were obtained from the hippocampi of E-18 day Sprague-Dawley fetal rat pups. Isolated hippocampi were gently dissociated by trypsin (0.05%), followed by triturated in HBSS and centrifuged at 1000 rpm. Cell pellets were resuspended in Neurobasal medium with B-27 supplement, GlutaMAX, L-glutamic acid (12.5×10^{-6} M), and penicillin-streptomycin (1%). Dissociated neurons were seeded on a laminin-coated SiMC array at a density of 100 cells mm^{-2} and incubated at 37 °C and 5% CO_2. This study was approved by the IACUC (Institutional Animal Care and Use Committee) of KAIST.

Immunocytochemistry and Live Cell Imaging: *a) Immunocytochemistry*: Cultured primary hippocampal neurons were fixed in 4% paraformaldehyde and 2% glutaraldehyde solution for 10 min and washed three times with PBS for 5 min each. The fixed samples were immersed in 0.1% Triton X-100 for 10 min followed by washing with PBS, and nonspecific binding was blocked by 6% BSA for 30 min. The cytoskeletal structures of neurons were stained by treating the samples with anti-β-tubulin III in a 1.5% BSA solution overnight at 4 °C, followed by the addition of secondary antibodies and Alexa Fluor 488 phalloidin for 1 h. Samples were mounted on sterilized glass slides with mounting solution containing DAPI.

b) Real-Time Imaging: Primary hippocampal neurons were immersed in serum-free medium containing 25×10^{-6} M NeuO after 30 min incubation for stable adhesion. The nuclei of neurons were stained by 10×10^{-6} M Hoechst 33342 for 5 min, followed by washing three times with media at 3 h of in vitro culture. Fluorescent images of the neurons were taken with a confocal laser-scanning microscope (LSM 800, Carl Zeiss) every 15 min from 4 to 12 h of culture.

Quantification of Neurite Length/Directionality and Neuronal Migration: Neurite lengths and directions were measured by using the NeuronJ plugin, and the movement of neurons was tracked by using the TrackMate plugin for Fiji software (NIH).

FE-SEM Imaging: Cultured primary hippocampal neurons were fixed in 2% glutaraldehyde solution for 30 min. After washing with PBS, the graded series of water–ethanol mixture solutions (25%, 50%, 75%, 90%, 95%, and 99%) were prepared to dehydrate the samples. Samples were immersed in each solution for 5 min, and the dehydration in 99% ethanol

solution was repeated three times. The dehydrated samples were immersed in HMDS for 10 min and dried overnight at a fume hood. Dried samples were sputter-coated with platinum for SEM imaging (Hitachi S-4800).

Statistical Analysis: The values of microcone pitches were expressed as mean ± standard deviation (SD). The sample size (n) and significance level were presented in the figure legend for each statistical analysis. The probability value of $p < 0.05$ was considered significantly different.

Supporting Information

Supporting Information is available from the Wiley Online Library or from the author.

Acknowledgements

This work was supported by the Basic Science Research Program through the National Research Foundation of Korea (NRF) funded by the Ministry of Science, ICT & Future Planning (MSIP 2012R1A3A2026403), and "HELLAS-CH" (MIS Grant No. 5002735) which was implemented under the "Action for Strengthening Research and Innovation Infrastructures," funded by the Operational Program "Competitiveness, Entrepreneurship and Innovation" (NSRF 2014–2020) and co-financed by Greece and the European Union (European Regional Development Fund). The authors would like to thank A. Manousaki for SEM images.

Conflict of Interest

The authors declare no conflict of interest.

Keywords

hippocampal neurons, microcone arrays, neurite elongation, neuronal migration, topography

Received: April 10, 2020
Revised: June 22, 2020
Published online: August 20, 2020

[1] M. E. Hatten, *Annu. Rev. Neurosci.* **1999**, *22*, 511.
[2] H. T. Ghashghaei, C. Lai, E. S. Anton, *Nat. Rev. Neurosci.* **2007**, *8*, 141.
[3] C. G. Silva, E. Peyre, L. Nguyen, *Nat. Rev. Neurosci.* **2019**, *20*, 318.
[4] P. Rakic, *J. Comp. Neurol.* **1972**, *145*, 61.
[5] B. Nadarajah, J. E. Brunstrom, J. Grutzendier, R. O. Wong, A. L. Pearlman, *Nat. Neurosci.* **2001**, *4*, 143.
[6] P. Rakic, *J. Comp. Neurol.* **1971**, *141*, 283.
[7] P. Weiss, *J. Exp. Zool.* **1934**, *68*, 393.
[8] N. A. O'Rourke, M. E. Dailey, S. J. Smith, S. K. McConnell, *Science* **1992**, *258*, 299.
[9] J. G. Corbin, S. Nery, G. Fishell, *Nat. Neurosci.* **2001**, *4*, 1177.
[10] M. Oscar, J. L. R. Rubenstein, *Nat. Rev. Neurosci.* **2001**, *2*, 780.
[11] H. Wichterle, J. M. Garcia-Verdugo, A. Alvarez-Buylla, *Neuron* **1997**, *18*, 779.
[12] G. J. Sun, Y. Zhou, R. P. Stadel, J. Moss, J. H. A. Yong, S. Ito, N. K. Kawasaki, A. T. Phan, J. H. Oh, N. Modak, R. R. Reed, N. Toni, H. Song, G.-l. Ming, *Proc. Natl. Acad. Sci. USA* **2015**, *112*, 9484.
[13] S. P. Khan, G. G. Auner, G. M. Newaz, *Nanomedicine* **2005**, *1*, 125.
[14] V. Brunetti, G. Maiorano, L. Rizzello, B. Sorce, S. Sabella, R. Cingolani, P. P. Pompa, *Proc. Natl. Acad. Sci. USA* **2010**, *107*, 6264.
[15] W. K. Cho, K. Kang, G. Kang, M. J. Jang, Y. Nam, I. S. Choi, *Angew. Chem., Int. Ed.* **2010**, *49*, 10114.
[16] G. Piret, M.-T. Perez, C. N. Prinz, *Biomaterials* **2013**, *34*, 875.
[17] C. Prinz, W. Hällström, T. Mårtensson, L. Samuelson, L. Montelius, M. Kanje, *Nanotechnology* **2008**, *19*, 345101.
[18] M. Park, E. Oh, J. Seo, M.-H. Kim, H. Cho, J. Y. Choi, H. Lee, I. S. Choi, *Small* **2016**, *12*, 1148.
[19] V. Onesto, L. Cancedda, M. L. Coluccio, M. Nanni, M. Pesce, N. Malara, M. Cesarelli, E. Di Fabrizio, F. Amato, F. Gentile, *Sci. Rep.* **2017**, *7*, 9841.
[20] S. Kuddannaya, C. S. Tong, Y. Fan, Y. Zhang, *Adv. Mater. Interfaces* **2018**, *5*, 1700819.
[21] K. Kang, M.-H. Kim, M. Park, I. S. Choi, *J. Nanosci. Nanotechnol.* **2014**, *14*, 513.
[22] M.-H. Kim, M. Park, K. Kang, I. S. Choi, *Biomater. Sci.* **2014**, *2*, 148.
[23] C. Simitzi, A. Ranella, E. Stratakis, *Acta Biomater.* **2017**, *51*, 21.
[24] A. Rajnicek, S. Britland, C. McCaig, *J. Cell Sci.* **1997**, *110*, 2905.
[25] A. T. Nguyen, S. R. Sathe, E. K. F. Yim, *J. Phys.: Condens. Matter* **2016**, *28*, 183001.
[26] N. Gomez, Y. Lu, S. Chen, C. E. Schmidt, *Biomaterials* **2007**, *28*, 271.
[27] B. W. Tuft, L. Xu, S. P. White, A. E. Seline, A. M. Erwood, M. R. Hansen, C. A. Guymon, *ACS Appl. Mater. Interfaces* **2014**, *6*, 11265.
[28] K. Kang, S.-E. Choi, H. S. Jang, W. K. Cho, Y. Nam, I. S. Choi, J. S. Lee, *Angew. Chem., Int. Ed.* **2012**, *51*, 2855.
[29] T. Wu, J. Xue, Y. Xia, *Angew. Chem., Int. Ed.* , , https://doi.org/10.1002/anie.202002593.
[30] M. Antman-Passig, S. Levy, C. Gartenberg, H. Schori, O. Shefi, *Tissue Eng., Part A* **2017**, *23*, 403.
[31] J. S. Chua, C.-P. Chng, A. A. K. Moe, J. Y. Tann, E. L. K. Goh, K.-H. Chiam, E. K. F. Yim, *Biomaterials* **2014**, *35*, 7750.
[32] K. Kang, Y.-S. Park, M. Park, M. J. Jang, S.-M. Kim, J. Lee, J. Y. Choi, D. H. Jung, Y.-T. Chang, M.-H. Yoon, J. S. Lee, Y. Nam, I. S. Choi, *Nano Lett.* **2016**, *16*, 675.
[33] C. Leclech, M. Renner, C. Villard, C. Métin, *Biomaterials* **2019**, *214*, 119194.
[34] B. T. Schaar, S. K. McConnell, *Proc. Natl. Acad. Sci. USA* **2005**, *102*, 13652.
[35] H. Umeshima, T. Hirano, M. Kengaku, *Proc. Natl. Acad. Sci. USA* **2007**, *104*, 16182.
[36] D. J. Solecki, N. Trivedi, E. E. Govek, R. A. Kerekes, S. S. Gleason, M. E. Hatten, *Neuron* **2009**, *63*, 63.
[37] A. Bellion, J.-P. Baudoin, C. Alvarez, M. Borenens, C. Métin, *J. Neurosci.* **2005**, *25*, 5691.
[38] J.-W. Tsai, K. H. Bremner, R. B. Vallee, *Nat. Neurosci.* **2007**, *10*, 970.
[39] K. Baranes, D. Hibsh, S. Cohen, T. Yamin, S. Efroni, A. Sharoni, O. Shefi, *Nano Lett.* **2019**, *19*, 1451.
[40] D. H. Kim, K. Han, K. Gupta, K. W. Kwon, K. Y. Suh, A. Levchenko, *Biomaterials* **2009**, *30*, 5433.
[41] X. Sun, M. K. Driscoll, C. Guven, S. Das, C. A. Parent, J. T. Fourkas, W. Losert, *Proc. Natl. Acad. Sci. USA* **2015**, *112*, 12557.
[42] Q. Y. Tang, W. X. Qian, Y. H. Xu, S. Gopalakrishnan, J. Q. Wang, Y. W. Lam, S. W. Pang, *J. Biomed. Mater. Res.* **2015**, *103*, 2383.
[43] M. Arnold, V. C.Hirschfeld-Warneken, T. Lohmüller, P. Heil, J. Blümmel, E. A. Cavalcanti-Adam, M. López-García, P. Walther, H. Kessler, B. Geiger, J. P. Spatz, *Nano Lett.* **2008**, *8*, 2063.
[44] D. H. Kim, C. H. Seo, K. Han, K. W. Kwon, A. Levchenko, K. Y. Suh, *Adv. Funct. Mater.* **2009**, *19*, 1579.
[45] I. Paradisanos, C. Fontakis, S. H. Anastasiadis, E. Stratakis, *Appl. Phys. Lett.* **2015**, *107*, 111603.
[46] A. Ranella, M. Barberoglou, S. Bakogianni, C. Fontakis, E. Stratakis, *Acta Biomater.* **2010**, *6*, 2711.
[47] A. L. Calof, A. D. Lander, *J. Cell Biol.* **1991**, *115*, 779.

[48] A. Faissner, J. Reinhard, *Glia* **2015**, *63*, 1330.
[49] F. J. Martini, M. Valiente, G. L. Bendito, G. Szabó, F. Moya, M. Baldeolmillos, O. Marin, *Development* **2009**, *136*, 41.
[50] F. C. de Anda, A. Gärtner, L.-H. Tsai, C. G. Dotti, *J. Cell Sci.* **2008**, *121*, 178.
[51] O. Marin, M. Valiente, X. Ge, L.-H. Tsai, *Cold Spring Harbor Perspect. Biol.* **2010**, *2*, a001834.
[52] B. Nadarajah, J. G. Parnavelas, *Nat. Rev. Neurosci.* **2002**, *3*, 423.
[53] R. Ayala, T. Shu, L.-H. Tsai, *Cell* **2007**, *128*, 29.
[54] C. Simitzi, P. Efstathopoulos, A. Kourgiantaki, A. Ranella, I. Charalampopoulos, C. Fotakis, I. Athanassakis, E. Stratakis, A. Gravanis, *Biomaterials* **2015**, *67*, 115.
[55] J. C. Er, C. Leong, C. L. Teoh, Q. Yuan, P. Merchant, M. Dunn, D. Sulzer, D. Sames, A. Bhinge, D. Kim, S.-M. Kim, M.-H. Yoon, L. W. Stanton, S. H. Je, S.-W. Yun, Y.-T. Chang, *Angew. Chem., Int. Ed.* **2015**, *54*, 2442.
[56] J. A. Cooper, *Trends Neurosci.* **2008**, *31*,113.
[57] K. Hayashi, K.-i. Kubo, A. Kitazawa, K. Nakajima, *Front. Neurosci.* **2015**, *9*, 135.
[58] M. E. Ward, H. Jiang, Y. Rao, *Mol. Cell. Neurosci.* **2005**, *30*, 378.
[59] D. H. Tanaka, M. Yanagida, Y. Zhu, S. Mikami, T. Nagasawa, J.-i. Miyazaki, Y. Yanagawa, K. Obata, F. Murakami, *J. Neurosci.* **2009**, *29*, 1300.
[60] M. Yanagida, R. Miyoshi, R. Toyokuni, Y. Zhu, F. Murakami, *Proc. Natl. Acad. Sci. USA* **2012**, *109*, 16737.
[61] J. Seo, J. Kim, S. Joo, J. Y. Choi, K. Kang, W. K. Cho, I. S. Choi, *Small* **2018**, *14*, 1801763.
[62] C. Xie, L. Hanson, W. Xie, Z. Lin, B. Cui, Y. Cui, *Nano Lett.* **2010**, *10*, 4020.
[63] S. C. Noctor, V. Martínez-Cerdeño, L. Ivic, A. R. Kriegstein, *Nat. Neurosci.* **2004**, *7*, 136.
[64] Z. Xu, P. Fang, B. Xu, Y. Lu, J. Xiong, F. Gao, X. Wang, J. Fan, P. Shi, *Nat. Commun.* **2018**, *9*, 4745.
[65] A. Kitazawa, K.-i. Kubo, K. Hayashi, Y. Matsunaga, K. Ishii, K. Nakajima, *J. Neurosci.* **2014**, *34*, 1115.
[66] K. Kang, S. Y. Yoon, S.-E. Choi, M.-H. Kim, M.-H. Kim, M. Park, Y. Nam, J. S. Lee, I. S. Choi, *Angew. Chem., Int. Ed.* **2014**, *53*, 6075.
[67] D. Hoffman-Kim, J. A. Mitchel, R. V. Bellamkonda, *Annu. Rev. Biomed. Eng.* **2010**, *12*, 203.
[68] J. Seo, W. Youn, J. Y. Choi, H. Cho, H. Choi, C. Lanara, E. Stratakis, I. S. Choi, *Dev. Neurobiol.* https://doi.org/10.1002/dneu.22749.